



HAL
open science

Contrasting conduction mechanisms of two internal barrier layer capacitors: (Mn, Nb)-doped SrTiO₃ and CaCu₃Ti₄O₁₂

Kosuke Tsuji, Wei-Ting Chen, Hanzheng Guo, Wen-Hsi Lee, Sophie Guillemet, Clive A. Randall

► **To cite this version:**

Kosuke Tsuji, Wei-Ting Chen, Hanzheng Guo, Wen-Hsi Lee, Sophie Guillemet, et al.. Contrasting conduction mechanisms of two internal barrier layer capacitors: (Mn, Nb)-doped SrTiO₃ and CaCu₃Ti₄O₁₂. *Journal of Applied Physics*, 2017, 121 (6), pp.064107. 10.1063/1.4976011. hal-02403341

HAL Id: hal-02403341

<https://hal.science/hal-02403341>

Submitted on 10 Dec 2019

HAL is a multi-disciplinary open access archive for the deposit and dissemination of scientific research documents, whether they are published or not. The documents may come from teaching and research institutions in France or abroad, or from public or private research centers.

L'archive ouverte pluridisciplinaire **HAL**, est destinée au dépôt et à la diffusion de documents scientifiques de niveau recherche, publiés ou non, émanant des établissements d'enseignement et de recherche français ou étrangers, des laboratoires publics ou privés.



Open Archive Toulouse Archive Ouverte (OATAO)

OATAO is an open access repository that collects the work of Toulouse researchers and makes it freely available over the web where possible

This is an author's version published in: <http://oatao.univ-toulouse.fr/24482>

Official URL: <https://doi.org/10.1063/1.4976011>

To cite this version:

Tsuji, Kosuke and Chen, Wei-Ting and Guo, Hanzheng and Lee, Wen-Hsi and Guillemet, Sophie  and Randall, Clive A. *Contrasting conduction mechanisms of two internal barrier layer capacitors: (Mn, Nb)-doped SrTiO₃ and CaCu₃Ti₄O₁₂*. (2017) *Journal of Applied Physics*, 121 (6). 064107. ISSN 0021-8979

Any correspondence concerning this service should be sent to the repository administrator: tech-oatao@listes-diff.inp-toulouse.fr

Contrasting conduction mechanisms of two internal barrier layer capacitors: (Mn, Nb)-doped SrTiO₃ and CaCu₃Ti₄O₁₂

Kosuke Tsuji,^{1,a)} Wei-Ting Chen,^{1,2} Hanzheng Guo,¹ Wen-Hsi Lee,² Sophie Guillemet-Fritsch,³ and Clive A. Randall¹

¹ Center for Dielectrics and Piezoelectrics, Materials Research Institute, Department of Material Science and Engineering, The Pennsylvania State University, University Park, Pennsylvania 16802, USA

² Department of Electrical Engineering, National Cheng Kung University, Taiwan, No. 1, University Road, Tainan City 701, Taiwan

³ Laboratoire CIRIMAT, UMR CNRS5085, Université de Toulouse, 118 route de Narbonne 31062, Toulouse Cedex 9, France

The d.c. conduction is investigated in the two different types of internal barrier layer capacitors, namely, (Mn, Nb)-doped SrTiO₃ (STO) and CaCu₃Ti₄O₁₂ (CCTO). Scanning electron microscopy (SEM) and Capacitance - Voltage (*C-V*) analysis are performed to estimate the effective electric field at a grain boundary, E_{GB} . Then, the d.c. conduction mechanism is discussed based on the J (Current density)- E_{GB} characteristics. Three different conduction mechanisms are successively observed with the increase of E_{GB} in both systems. In (Mn, Nb)-doped STO, non-linear J - E_{GB} characteristics is temperature dependent at the intermediate E_{GB} and becomes relatively insensitive to the temperature at the higher E_{GB} . The J - E_{GB} at each regime is explained by the Schottky emission (SE) followed by Fowler-Nordheim (F-N) tunneling. Based on the F-N tunneling, the breakdown voltage is then scaled by the function of the depletion layer thickness and Schottky barrier height at the average grain boundary. The proposed function shows a clear linear relationship with the breakdown. On the other hand, F-N tunneling was not observed in CCTO in our measurement. Ohmic, Poole-Frenkel (P-F), and SE are successively observed in CCTO. The transition point from P-F and SE depends on E_{GB} and temperature. A charge-based deep level transient spectroscopy study reveals that 3 types of trap states exist in CCTO. The trap one with $E_t \sim 0.65$ eV below the conduction band is found to be responsible for the P-F conduction. *Published by AIP Publishing.*

[<http://dx.doi.org/10.1063/1.4976011>]

I. INTRODUCTION

A colossal permittivity (CP, $\epsilon' > 10^4$) in ceramic capacitors is often attributed to internal barrier layer capacitors (IBLC). While IBLCs act as a series of small capacitor in the material, achieving CP, they also act as potential barriers between adjacent *n*-type grains, which are responsible for the nonlinear current-voltage (*I-V*) characteristics. A Double Schottky Barrier (DSB) model is widely used to explain the capacitor-varistor multifunctional property of the IBLCs. The DSBs are formed by a deep electronic trap between interface of the *n*-type grains causing a band bending of conduction band across the grain boundary with the electron depletion layer.^{1,2} In many titanate systems, the main contribution to CP is associated with the IBLCs at grain boundaries.³⁻⁵ On the other hand, some other effects, such as a relaxation of defect complex^{6,7} and electrode-sample interface effect,^{8,9} have additionally been proposed to be a major contribution to CP in CaCuTiO₃ (CCTO) while the IBLC is also reported.^{5,10-12} The dominance of such effects is often sensitive to heat treatment conditions. It was demonstrated when CCTO is sintered above $\sim 1050^\circ\text{C}$, segregation of secondary layers is promoted and then IBLCs become dominant due to the increase of grain

boundary resistance.^{13,14} Thus, CP of CCTO can also be associated with IBLCs at the grain boundaries when the sintering temperature is sufficiently high. More detailed discussion on the nature of IBLs in CCTO can be found in Refs. 15-18.

For the varistor properties, many studies have been performed in doped-SrTiO₃ (STO) and CCTO by the impedance spectroscopy^{10,19} and *I-V* measurement with bicrystals^{20,21} and microelectrodes^{22,23}. It has been clearly shown that they have a IBLC structure: the grain boundaries are much more resistive than the *n*-type grains, and the non-linear *I-V* characteristics is associated with the grain boundaries. Thus, "Grain boundary limited current (GBLC)" is expected for the d.c. conduction in the IBLC bulk ceramics. Despite GBLC having been investigated in some ferroelectric thin film devices,^{24,25} few GBLC studies have been reported for the IBLC bulk ceramics.

Since the grain boundaries are very resistive, theoretical expressions for the leakage current in the dielectrics may be applicable for the GBLC. Fig. 1 shows a schematic description for the possible conduction across the DSB. The current flow across the DSB, as shown in Fig. 1(a), is a Schottky emission (SE) current, which can be expressed as²⁶

$$J = A^* T^2 \exp\left(\frac{\beta E^{1/2} - q\phi_B}{kT}\right) \left\{ 1 - \exp\left(-\frac{qV}{kT}\right) \right\}, \quad (1)$$

^{a)} Author to whom correspondence should be addressed. Electronic mail: tuk152@psu.edu. Fax: 1 814 865 7173

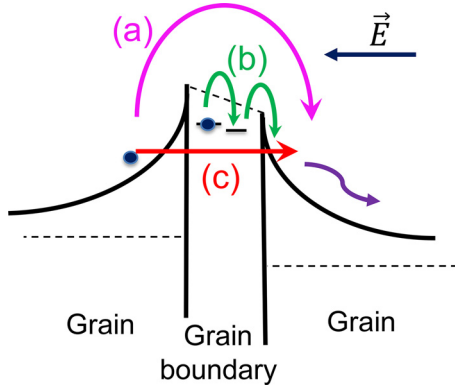


FIG. 1. Leakage current mechanism across the double Schottky barrier at a grain boundary. (a) Schottky emission (b) Poole Frenkel emission (c) Fowler Nordheim tunneling.

where T is the absolute temperature and E is the electric field between electrodes, A^* is the effective Richardson constant, ϕ_B is the Schottky barrier height, k is the Boltzmann constant, q is the electric charge, and V is applied voltage. When the applied voltage is sufficiently large, Eq. (1) can be expressed as²⁶⁻²⁸

$$J \propto T^2 \exp\left[\frac{\beta E^{1/2} - q\phi_B}{kT}\right]. \quad (2)$$

Though Eq. (2) is often used to describe the electrode-limited conduction, it is also used for d.c. conduction through the DSB.^{11,29} The Poole-Frenkel (P-F) conduction mechanism is also possible if the electron trap centers exist at the DSB interfaces. For the GBLC, it can be interpreted as a field-assisted thermally hopping process as shown in Fig. 1(b). The P-F conduction can be expressed as²⁶⁻²⁸

$$J \propto E \exp\left[\frac{\beta E^{1/2} - q\phi_t}{kT}\right], \quad (3)$$

where ϕ_t is the trap level at the insulating layer. Whether SE or P-F can be determined by the slope ($=\beta/kT$) in the SE plot ($\ln(J/T^2)$ vs \sqrt{E}) and P-F plot ($\ln(J/E)$ vs \sqrt{E}). The β in Eqs. (2) and (3) can be expressed as²⁶⁻²⁸

$$\beta = \sqrt{\frac{q^3}{\eta\pi\epsilon_0\epsilon_\infty}}, \quad (4)$$

where ϵ_0 is the vacuum permittivity, and ϵ_∞ is the dynamic permittivity ($\equiv n^2$). n is refractive index for STO and CCTO. Then, η can be extracted from the slope of a SE and P-F plot. The SE should give the $\eta_{SE} = 4$ while the PF should give a $\eta_{PF} = 1$. When high voltage is applied, electrons could tunnel through the DSB as shown in Fig. 1(c). It can be expressed by Fowler-Nordheim (F-N) tunneling equation^{26,28}

$$J \propto E^2 \exp(-\gamma/E) \\ \gamma = \frac{8\pi\sqrt{2m^*}}{3qh} (q\phi_B)^{3/2}, \quad (5)$$

where h is the Planck constant, and m^* is the effective mass of tunneling. The F-N tunneling through the DSB was observed in ZnO varistors.³⁰ What is quite different from SE

and P-F is that F-N tunneling is a temperature independent process. Furthermore, a linear relationship should be shown in the F-N plot ($\ln(J/E^2)$ vs $1/E$).

The conduction analyses in STO and CCTO system are mostly reported in thin film devices. The SE is dominant in STO thin film³¹ and both SE and PF could be dominant in CCTO thin film depending on the sample thickness.³² But it should be quite different in the IBLC system due to the large contribution from the grain boundaries. The difficulty for the d.c. conduction analysis on IBLC bulk ceramics originates from the inhomogeneous microstructure, and therefore field distributions. Since the resistivity of the grain boundaries is much higher than that of the grain, the leakage current, J , in Eqs. (2), (3), and (5) should be expressed in terms of the “local electric field” at a GB, E_{GB} , instead of an average electric field, E (\therefore voltage per electrode distance). The use of E would therefore not give a reasonable value of η and γ in Eqs. (4) and (5). An estimation for the E_{GB} should be essential for the GBLC analysis.

The objective of our study is to provide a methodology to better understand the nature of conduction in semiconductive polycrystalline materials. We exemplify this with an investigation of J vs E_{Ele} characteristics of IBLCs in the (Nb, Mn)-doped STO and CCTO. Both systems were confirmed to have an IBLC structure in our previous studies.^{33,34} The E_{GB} is estimated by a combination of SEM and C - V analyses. The d.c. conduction mechanisms are discussed based on Eqs. (1) (5). Charge-based deep level transition spectroscopy (Q-DLTS) is performed to investigate the trap state at the DSBs. There is also an extended discussion for the important properties such as the breakdown voltage and non-linearity, and the electronic trap center is also demonstrated and quantified.

II. EXPERIMENTAL PROCEDURE

The (1%Mn + 0.6%Nb)-doped STO single layer capacitors were manufactured by a 2-step tape fabricating procedure used in our previous work.³³ The green chips (5 mm \times 3.5 mm) were sintered at 1400 °C for 5 h in N_2 gas. The as-sintered samples underwent a reoxidation at 1200 °C for 20 min to 10 h.

CCTO powders were synthesized by the soft chemistry method of co-precipitation followed by a calcination treatment.³⁵ The CCTO thick films were realized by tape casting method and the monolayers of CCTO film were stacked with screen printed Ag/Pd electrodes. More detailed process can be found in the previous work.³⁴ After thermo-compression and binder removal, the specimen was sintered in air at 1100 °C for 24 h. The final device component (dimensions 6.2 \times 6.4 mm²), contains 10 interdigitated internal electrodes. The terminations, made of pure Ag, were applied by screen printing and post-fired at 700 °C during 20 min.

The microstructure of specimens was observed by Scanning Electron Microscopy (ESEM, FEI, Hillsboro, OR) for the (1%Mn + 0.6%Nb)-doped STO and Field Emission SEM (Merlin, Carl Zeiss Microscopy LLC., Thornwood, NY) for CCTO. The cross section of CCTO was polished and then thermally etched at 1000 °C for 30 min before the

FESEM analysis. The average grain size was estimated using Nano measure software and SmartTiff, V3 (Carl Zeiss SMT) for the (1%Mn + 0.6%Nb)-doped STO and CCTO, respectively. The capacitance of the samples was measured using a precision LCR meter (HP 4284 A, Hewlett-Packard, Palo Alto, CA) at room temperature. The d.c. current (I) voltage (V) characteristics was measured with the pA meter (HP 4140B, Hewlett Packard, Palo Alto, CA). The d.c. field is applied for 1 min, and the current was recorded every 3 s. Because it was proposed that Joule self-heating could greatly alter the I - V characteristics of CCTO,³⁶ the voltage applied was removed for 30 s at each step. The 30 s interval was confirmed to be enough by comparing the I - V characteristics with 30 and 180 s of the interval. The Q -DLTS characterization was performed in a home-made charge measurement system.³⁷ The time resolution of the measurement was 4 μ s. The pulse voltage with a 0.8 V height and 100 μ s duration was applied as a charging voltage.

III. RESULTS AND DISCUSSION

A. SEM and C-V analysis on the CCTO and (1%Mn + 0.6%Nb)-doped STO

In order to estimate the E_{GB} , characterization with SEM and C - V measurements were performed. Figs. 2(a) and 2(b) show SEM images of (1%Mn + 0.6%Nb)-doped STO single layer ceramics annealed for 20 and 200 min. The average grain size, d , for these two samples is given as $15.5 \pm 3.7 \mu\text{m}$ and $15.8 \pm 3.7 \mu\text{m}$, respectively. Few differences are noted between two specimens, since the grain-growth occurred mainly during the sintering process. The annealing process, performed at 200 °C lower than the sintering treatment, did not affect the grain size. In this work, we assumed the d for

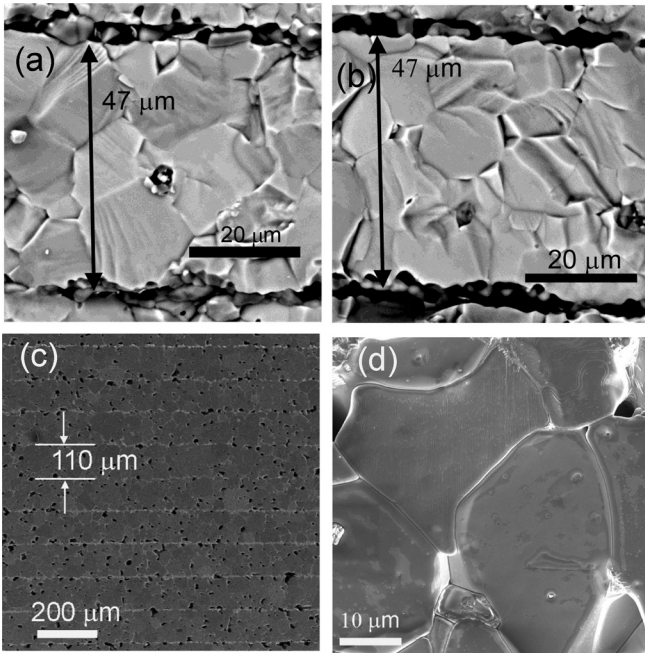


FIG. 2. SEM micrograph of (1%Mn + 0.6%Nb) doped STO ceramics annealed for (a) 20 min (b) 200 min. FESEM micrograph of CCTO MLCC: (c) 10 electrodes (d) Grain morphology.

the (1%Mn + 0.6%Nb)-doped STO samples (with different annealing times) to be $\sim 15 \mu\text{m}$. Figs. 2(c) and 2(d) show SEM images of CCTO MLCC. Fig. 2(c) shows a high quality CCTO MLCC, and the 10 electrodes are aligned in almost a parallel manner. Relatively larger grain sizes were observed in Fig. 2(d) compared to the (1%Mn + 0.6%Nb)-doped STO. The d for CCTO is calculated as $\sim 32.4 \pm 1.3 \mu\text{m}$.

The C - V analysis was carried out, and through assuming, we have DSB at the grain boundaries, the space charge capacitance should have a bias dependence characteristic. This can be described by Mukae's equation as follows:³⁸

$$\left(\frac{1}{C} - \frac{1}{2C_0}\right)^2 = \frac{2}{q\epsilon N_d}(\phi + V), \quad (6)$$

where C is the capacitance per unit area, q is the electronic charge, ϵ is the permittivity of the grain, N_d is the donor concentration in the grain, ϕ is the Schottky barrier height, and C_0 is the capacitance per unit area without the bias voltage. ϕ in (7) can also be described as

$$\phi = \frac{qN_s^2}{2\epsilon N_d}, \quad (7)$$

where the density of surface trap states (N_s) and depletion layer width (δ) can be estimated by

$$N_s = N_d \delta, \quad (8)$$

$(1/C - 1/2C_0)^2$ plot of CCTO is shown in Fig. 3. The $(1/C - 1/2C_0)^2$ plot demonstrates relatively a symmetric response for the positive and negative bias voltages, proving an excellent sample quality. From the slope and intercept of the linear regime, ϕ and N_d are calculated to be 0.80 eV and $2.9 \times 10^{19} \text{ cm}^{-3}$, respectively. Then N_s and δ are calculated to be $4.2 \times 10^{13} \text{ cm}^{-2}$, 15 nm based on Eqs. (7) and (8). The difference between the parameters extracted from positive and negative voltages is less than 6% for all the parameters. The summary of SEM and C - V measurement is shown in Table I with the dielectric properties measured at 1 kHz. The CP is confirmed in all the samples with relatively a low

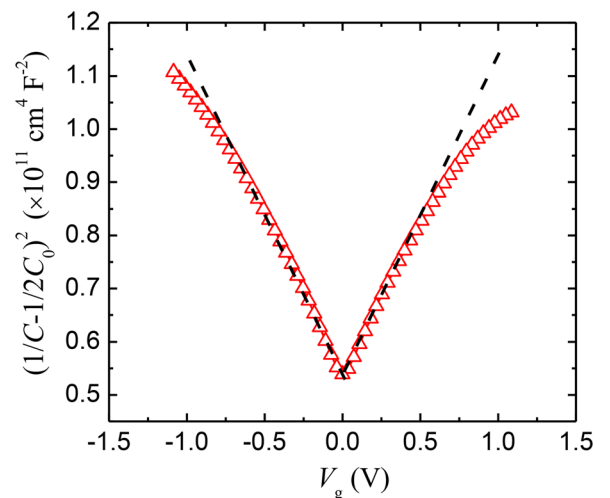


FIG. 3. $(1/C - 1/2C_0)^2$ plot of CCTO as a function of voltage per grain.

TABLE I. Summary of dielectric properties, average grain size, and depletion layer width.

Samples ^a	ϵ^b	$\tan \delta^b$	Average grain size, \bar{d} (μm) ^c	Depletion layer width, δ (nm) ^d
CCTO	1.1×10^4	0.14	32	15
STO50	6.0×10^4	0.049	15	30
STO100	3.7×10^4	0.030		37
STO200	2.7×10^4	0.027		51
STO600	2.0×10^4	0.018		69

^aSTO50 is meant to be (1%Mn + 0.6%Nb) doped STO annealed for 50 min.

^bDielectric properties were measured at 1 kHz at 298 K.

^cEstimated from SEM observations.

^dEstimated from $C-V$ analysis.

dielectric loss, $\tan \delta$. The $C-V$ result of (1%Mn + 0.6%Nb)-doped STO ceramics is reported in our previous work.³³

For the GBLC analysis, we proposed to use the E_{GB} , which is defined as the voltage drop per grain boundary. Since the grain is of n -type and the grain boundary is much more resistive, voltage drop at the grains can be neglected. Thus, E_{GB} can be approximated as

$$E_{GB} = \frac{\Delta V}{\delta} \approx \frac{V}{(L/d)\delta} = E \frac{d}{\delta}, \quad (9)$$

where d is the average grain size, δ is the depletion layer width, and ΔV is the voltage drop at depletion layer. The E_{GB} can be now estimated from the results of SEM and $C-V$ analysis. Then, GBLC for the IBLC bulk ceramics should be expressed by Eqs. (1)–(5) using E_{GB} instead of E based on the results outlined in Table I and using Eq. (9).

B. D. C. conduction analysis in the (1%Mn + 0.6%Nb)-doped SrTiO₃

Figs. 4(a)–4(d) show a temperature dependence of $J-E_{GB}$ characteristics in the (1%Mn + 0.6%Nb)-doped STO ceramics annealed for 50–600 min. Both the resistivity and the breakdown voltage increase with the increase of the annealing time. At the low E_{GB} , $J-E_{GB}$ characteristics follow the Ohm's law and then the non-linear $J-E_{GB}$ characteristics appear at the higher E_{GB} . The non-linear $J-E_{GB}$ characteristics in this regime (Pre-breakdown) is still temperature dependent. Since the SE and the P-F are both thermally

activated processes as shown in Eqs. (2) and (3), either one could be dominant in the prebreakdown regime in (1%Mn + 0.6%Nb)-doped STO ceramics. Interestingly, J at the high E_{GB} (breakdown regime) show few temperature dependencies in all the samples. This indicates that the F-N tunneling would be the dominant conduction mechanism across DSB based on Eq. (5). Indeed, the onset field of temperature independent regime in Fig. 4 is close to 10^5 V/mm, which is high enough for the transition from the SE to the F-N tunneling.³⁰

Figs. 5(a)–5(d) show the SE and P-F plot for the (1%Mn + 0.6%Nb)-doped STO ceramics annealed for 50–600 min. SE plot at the pre-breakdown regime clearly shows a linear relationship in all the samples. From the slope of SE plot, η at 298 K is calculated based on Eqs. (2) and (4) as 3.67, 2.08, 2.85, and 3.08 for the samples annealed for 50, 100, 200, and 600 min as shown in Table II. Here, ϵ_∞ ($\equiv n^2$) = 5.78 was used.³⁹ The values of η extracted from the SE plot are reasonably close to the theoretical value, $\eta_{SE} = 4$. On the other hand, the value of η at 298 K calculated from the slope in the P-F plot were 23.3, 8.36, 9.29, and 10.45 for the sample annealed for 50, 100, 200, and 600 min, respectively. They are almost one order higher than the theoretical value, $\eta_{PF} = 1$. The discrepancy between η from SE and P-F is maintained from 218 to 298 K as shown in Table II. Also, the linear relationship in the PF plot is limited in a shorter regime, compared to, in the SE plot. Therefore, the SE is suggested for the d.c. conduction of GBLC in the (1%Mn + 0.6%Nb)-doped STO ceramics in the prebreakdown regime. It is noted that the d.c. conduction is not controlled by neither the bulk shallow traps nor the Schottky barrier of electrode. We investigated the values of η from the conventional SE and P-F plot with using E instead of E_{GB} . The slopes in Fig. 5 with E give almost 10 times larger than those with E_{GB} for all specimens. The resulting value of η are found to be less than 0.01, which are far from $\eta_{PF} = 1$ and $\eta_{SE} = 4$. Thus, GBLC is likely instead of the bulk-limited P-F or electrode-limited SE. The SE over the DSB is then suggested. The SE is also able to describe the Ohmic regime. When the electric field is very small, the last term in Eq. (1) can be approximated as $\exp(-qV/kT) \approx (1 - qV/kT)$ and then the linear relationship can be deduced.⁴⁰ This is consistent with the Ohmic regime at the low E_{GB} regime. The Schottky barriers height can be estimated from the intercept in the SE plot based on Eq. (2) when $E \rightarrow 0$.

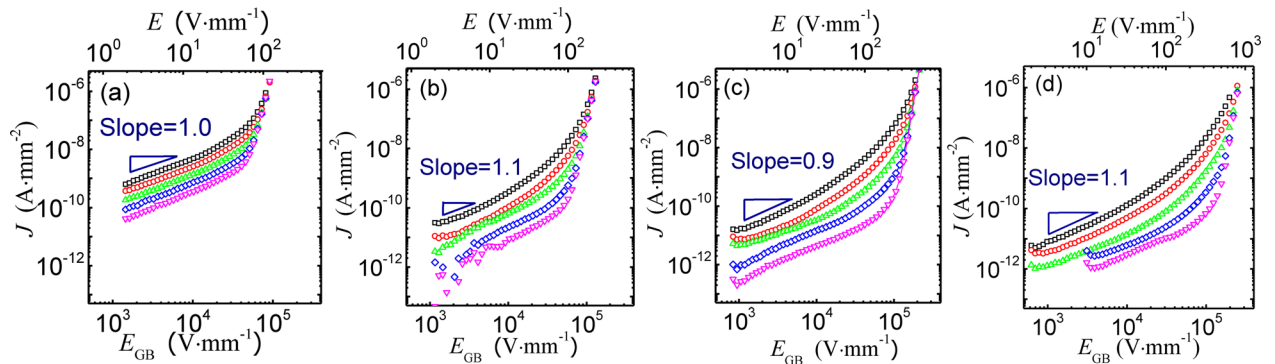


FIG. 4. $J-E_{GB}$ characteristics in the (1%Mn + 0.6%Nb) doped STO ceramics annealed for (a) 50 min (b) 100 min (c) 200 min and (d) 600 min at (□) 298 K, (○) 278 K, (△) 258 K, (◇) 238 K, and (▽) 218 K.

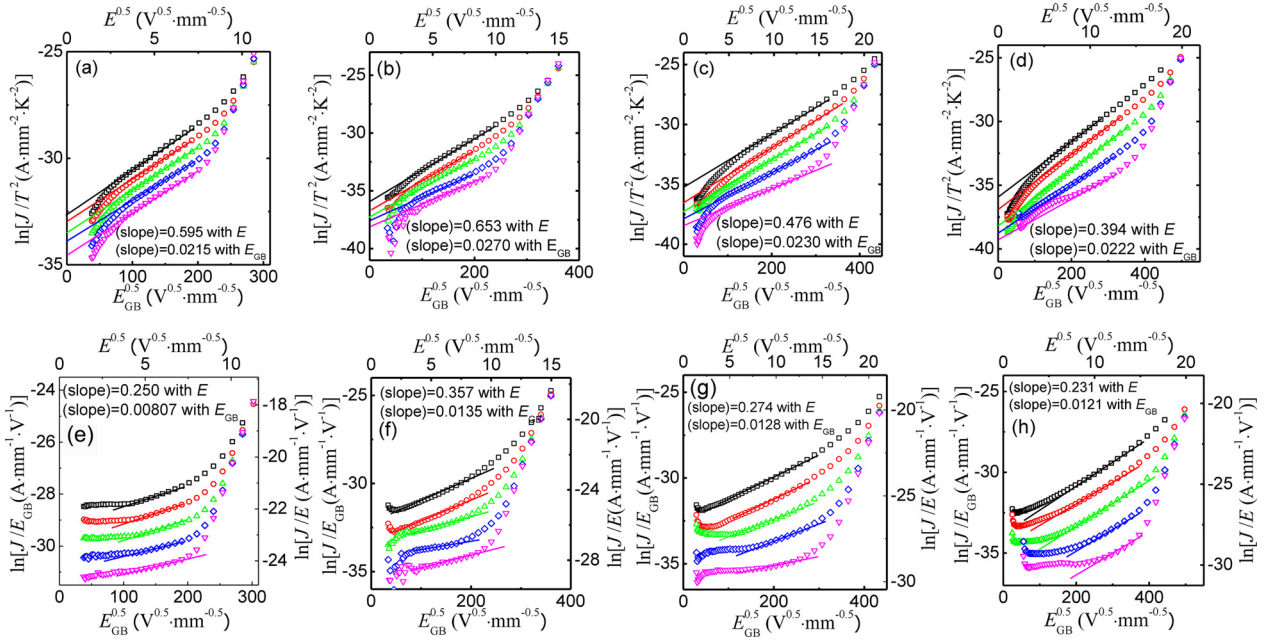


FIG. 5. SE (upper) and P F (bottom) plot of the (1%Mn + 0.6%Nb) doped STO ceramics annealed for (a), (d) 50 min (b), (f) 100 min (c), (g) 200 min and (d), (h) 600 min at (\square) 298 K, (\circ) 278 K, (\triangle) 258 K, (\diamond) 238 K, and (∇) 218 K. η The values of slopes at 298 K are shown for reference. The resulting η with E_{GB} in the other temperature range can be found in Table II. The value of η with E is mentioned in text.

TABLE II. The value of η extracted from P F and SE plot of the (1%Mn + 0.6%Nb) doped STO ceramics annealed for 50, 100, 200, and 600 min.

T (K)	(Mn, Nb) STO 50 min		(Mn, Nb) STO 100 min		(Mn, Nb) STO 200 min		(Mn, Nb) STO 600 min	
	η_{PF}	η_{SE}	η_{PF}	η_{SE}	η_{PF}	η_{SE}	η_{PF}	η_{SE}
298	23.3	3.67	8.36	2.08	9.29	2.85	10.5	3.08
278	27.6	4.08	11.2	3.36	11.9	3.22	11.9	3.70
258	39.8	4.15	27.7	4.00	18.6	4.40	12.9	4.29
238	56.8	4.73	66.9	6.02	33.9	6.40	21.3	6.04
218	82.5	5.88	55.8	6.97	126	11.6	25.5	12.0

Fig. 6 shows the Arrhenius plot of Eq. (2). ϕ_B is calculated to be 0.16, 0.17, 0.24, and 0.31 eV for the samples annealed for 50, 100, 200, and 600 min, respectively. It is shown that ϕ_B increased with the increase of annealing time as well as

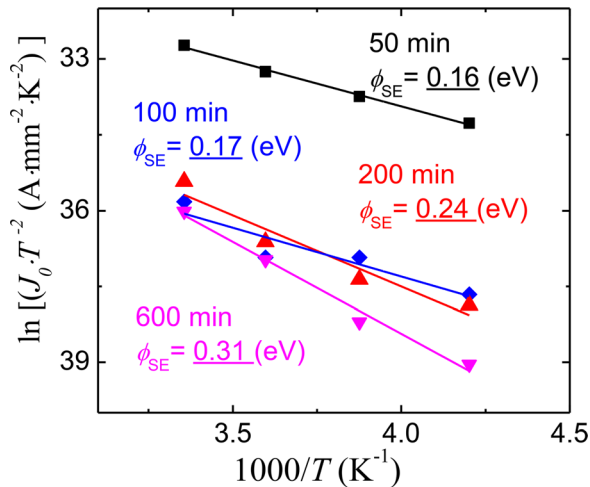


FIG. 6. The barrier height of (1%Mn + 0.6%Nb) doped STO ceramics annealed for 50, 100, 200, and 600 min, fitted by Eq. (2).

δ . These values in this work are smaller than the ones determined by C - V analysis in our previous work while the trend with the annealing time is maintained.³³ This is probably due to different values of permittivity with d.c. and a.c. measurement or barrier lowering by d.c. bias might give the smaller value of ϕ_B . Similar discrepancy of ϕ_B determined by C - V and SE plot has been reported in ZnO varistor⁴¹ and CCTO.⁴² In this work, the value of ϕ_B determined from the SE plot will be used for the measurement consistency of d.c. conduction.

As discussed in the J - E_{GB} characteristics shown in Fig. 4, the F-N tunneling is expected at the breakdown regime in the (1%Mn + 0.6%Nb)-doped STO. Fig. 7 shows a F-N plot near the breakdown regime. Clear straight lines suggest the F-N tunneling dominates the d.c. conduction at the high E_{GB} in all the (1%Mn + 0.6%Nb)-doped STO samples annealed for 50 to 600 min. The slopes in the linear regime, which correspond to γ in Eq. (5), also increase with the annealing time. Based on Eq. (5), ϕ_B is estimated as 0.13, 0.18, 0.29, and 0.32 eV for the samples annealed for 50, 100, 200, and 600 min. Here, an effective mass of the samples is assumed to be 4.8.⁴³ These values are then in good agreement with the ϕ_B extracted from the SE plot shown Fig. 6. Thus, it is

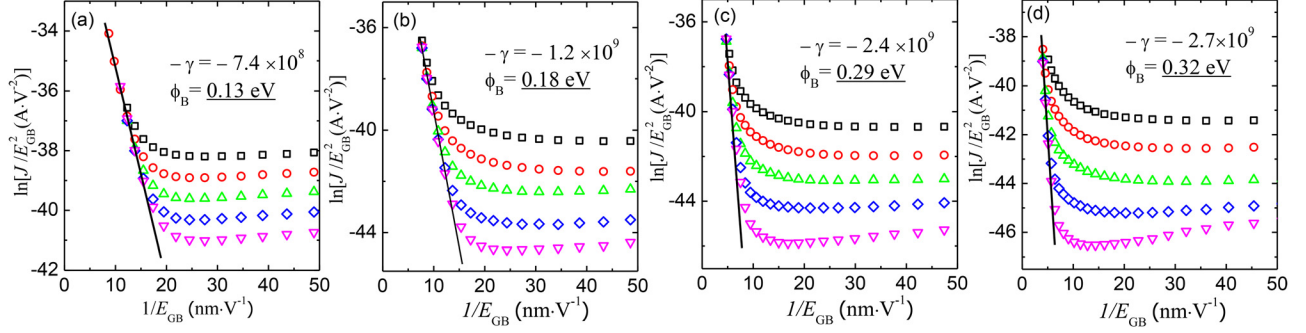


FIG. 7. F-N plot of the (1%Mn + 0.6%Nb) doped STO ceramics annealed for (a) 50 min (b) 100 min (c) 200 min, and (d) 600 min at (\square) 298 K, (\circ) 278 K, (\triangle) 258 K, (\diamond) 238 K, and (∇) 218 K.

likely that F-N tunneling was triggered at the critical field strength transition of the conduction mechanism from the SE controlled conduction. Therefore in summary, we consider the sudden increase of J in Fig. 4 is attributed to the F-N tunneling.

Prediction of a breakdown voltage is of interest for the designing operation voltage in IBLC and varistor materials. However, it is still difficult to estimate it even though the d.c. conduction at the breakdown regime has been suggested. This is because Eq. (5) is difficult to be analytically solved in terms of E_{GB} at a certain leakage current (e.g., $J \approx 1 \text{ mA/cm}^2$). Fig. 8 shows the relationship between the breakdown voltage and the annealing time. The breakdown voltage increases with the annealing time but not in a regular manner. So the precise value of the breakdown voltage cannot be easily extracted from the relationship with the annealing time. In principle, we can hypothesise that both the tunneling probability, which corresponds to an increase of J , and the transition point for F-N tunneling at the fixed temperature are determined by both ϕ_B and E_{GB} .⁴⁴ In the IBL systems, E_{GB} depends on δ as shown in Eq. (6). Therefore, in the (1%Mn + 0.6%Nb)-doped STO ceramics, those samples annealed with higher values of ϕ_B and δ should have a higher breakdown voltage because higher ϕ_B and thicker δ inhibit electrons to tunnel through the DSB. For this reason, we scale the breakdown voltage with $(\phi_B \times \delta)/2$, which

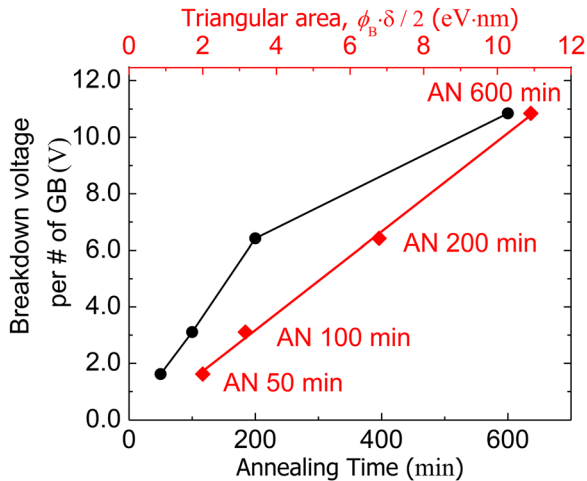


FIG. 8. The correlation between the breakdown voltage and annealing time and the area of the barrier at the grain boundary ($(\phi_B \times \delta)/2$).

schematically interprets as a triangular area of DSB. Fig. 8 shows that this hypotheses works extremely well showing a linear relationship between the breakdown voltage and the triangular area of DSB. From this relationship, it seems to be possible to predict the breakdown voltage of the (1%Mn + 0.6%Nb)-doped STO ceramics with different annealing times. Though more discussion for the relationship may be required, at least to a first order approximation, the use of two parameters, ϕ_B and δ , should be reasonable when F-N tunneling dominates at the breakdown regime.

C. D.C. conduction analysis in the CCTO

A high nonlinear coefficient, α , (>900)⁴⁵ for CCTO is also of great interest. However, the value of α could be altered by the measurement conditions due to the joule self-heating.^{36,46} In this study, 30 s of zero bias interval was set after each d.c. bias was applied to avoid the joule self-heating. Fig. 9(a) shows J - E_{GB} characteristics of CCTO with different holding times at 15, 30, and 60 s at $T = 298$ K. Few differences in the J - E_{GB} characteristics of CCTO were observed among the different holding times except where very large leakage current is observed. The nonlinear coefficient was found out to be $\alpha \sim 5.5$, where it is defined as $\alpha \equiv \log(J_1/J_2)/\log(E_1/E_2)$ and J_1 and J_2 were selected as 1 and 10 $\text{mA} \cdot \text{cm}^{-2}$, respectively, and E_1 and E_2 are the values of E_{GB} corresponding to J_1 and J_2 . The slight difference of α with different holding times is less than 3%. The α obtained in this study is close to some of previous studies.^{29,47,48} It is concluded that, at least in our study, CCTO shows the much lower α than the highest reported value.

Then, the temperature dependence of J - E_{GB} characteristics of CCTO was investigated. As can be seen in Fig. 9(b), the leakage current in the CCTO is thermally activated within the whole range of E_{GB} . Unlike in the (1%Mn + 0.6%Nb)-doped STO, temperature independent regime was not observed even where high leakage ($\sim 1 \text{ mA/mm}^2$) was observed. Then, F-N tunneling is not expected in CCTO based on Eq. (5). Instead, SE or P-F conduction may be responsible for the d.c. conduction. Figs. 9(c) and 9(d) show P-F and SE plot of CCTO, respectively. Two separate straight lines are shown in both plots suggesting that a different d.c. conduction mechanism may appear at lower (pre-breakdown regime) and higher E_{GB} (breakdown regime). Table III shows η from pre-breakdown and breakdown

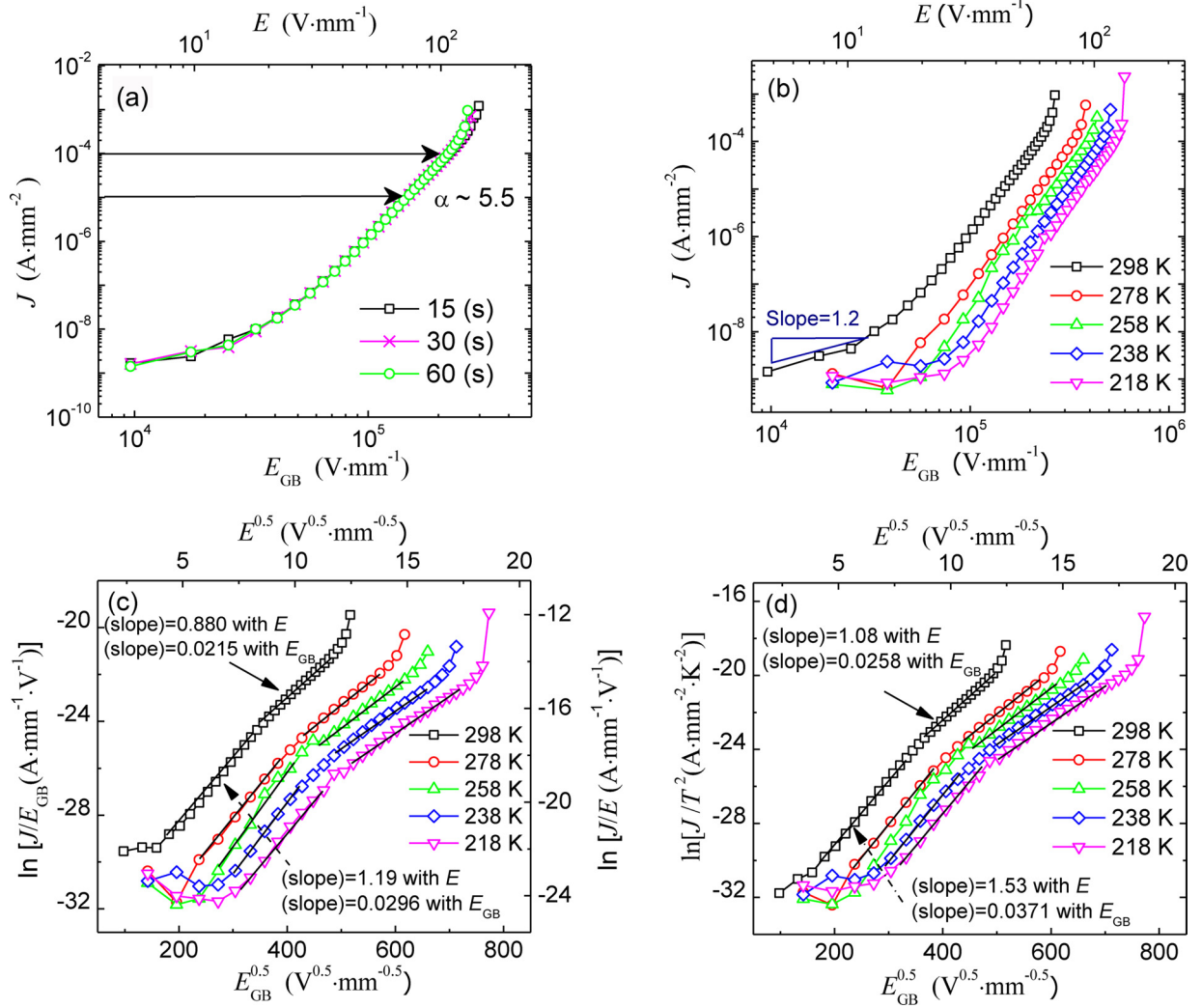


FIG. 9. (a) $J E_{GB}$ characteristics of CCTO at 298 K as a function of the holding time of voltage applied. (b) Temperature dependence of $J E_{GB}$ characteristics of CCTO (c) P F plot of CCTO (d) SE plot of CCTO. The values of slope at 298 K are shown in (c) and (d) for reference. The resulting η with E_{GB} in the other temperature range can be found in Table III. The η with E is mentioned in text.

regime in the P-F and SE plot. Here, $\epsilon_{\infty} = 6.0$ is assumed based on theoretical⁴⁹ and experimental⁵⁰ results. Over all the temperature range, η from the P-F plot at the pre-breakdown regime is closer to the theoretical value, $\eta_{PF} = 1$ than η from the P-F plot at the breakdown regime. The values of η from the SE plot do not follow $\eta_{SE} = 4$ in the pre-breakdown regime. Thus, we deduce that the P-F conduction dominates the conduction mechanism for GBLC at the pre-breakdown regime. It has been previously suggested that CaTiO_3 and TiO_2 could act as charge trapping centers for

TABLE III. The value of η extracted from P F and SE plot of CCTO at the Pre breakdown and Breakdown regime.

T (K)	η_{PF}		η_{SE}	
	Pre breakdown	Breakdown	Pre Breakdown	Breakdown
298	1.67	3.14	1.06	2.19
278	1.93	5.16	1.32	3.43
258	1.44	6.64	1.06	4.50
238	2.41	9.20	1.77	5.28
218	3.02	10.1	2.25	6.04

P-F emission in the CCTO systems.^{51–54} In addition, our previous study suggested that CaTiO_3 and TiO_2 secondary phases, as well as CuO phase, exist in CCTO.³⁴ In this study, one of those secondary phases located at the grain boundaries could be responsible for the P-F emission by forming the trap centers. The significance of the trap center will be discussed later. Then, the trap level is calculated from the temperature dependence of $\ln(J/E_{GB})$ at the certain E_{GB} value in the P-F regime. Fig. 10 shows the Arrhenius plot of P-F emission. With the selected E_{GB} , a $\phi_t \sim 0.65$ eV of trap state at the grain boundaries was derived from Eq. (3).

Next, the d.c. conduction mechanism at the breakdown regime is discussed. The change of slope from the P-F regime, and linear relationship in SE plot suggest that the SE is the dominant d.c. conduction mechanism at the breakdown regime. The η in the pre-breakdown regime is not close to $\eta_{SE} = 4$ as expected by the dominance of P-F emission at this regime. On the other hand, the values of η at the breakdown regime in Table III show a reasonable range of values, 2.19–6.04, for the SE conduction. Thus, the SE type conduction is dominant at the breakdown regime of CCTO. The transition from P-F to SE may be caused when electrons

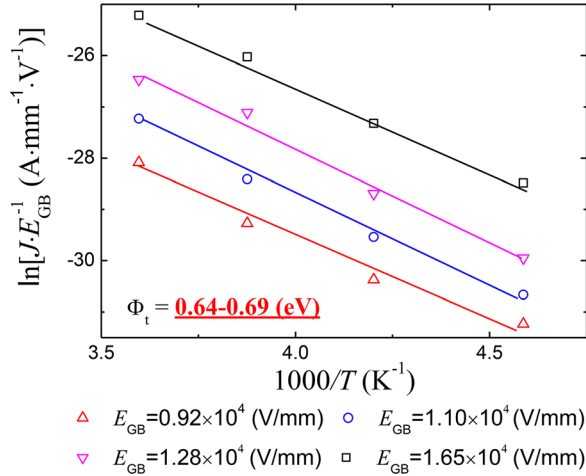


FIG. 10. Arrhenius plot of the P-F emission for the CCTO. The selected E_{GB} corresponds to the value at P-F emission regime shown in Fig. 6(c).

acquire enough energy to go over the DSB at the grain boundaries. This is consistent with the temperature and field dependence of the transition points in Figs. 9(c) and 9(d). The PF becomes less effective (or SE appears) at the lower E_{GB} with the higher temperature, which is probably because the electrons are thermally excited over the DSBs. As a result, three types of conduction, Ohmic, P-F, and SE are successively observed in the CCTO with the increase of E_{GB} . It is noted again that, the η turned out to be very small (<0.002) if E is used for the SE and PF plot instead of E_{GB} . This means that J - E_{GB} characteristics of CCTO with IBLC structure did not follow neither the well-known “bulk-limited” P-F emission nor “electrode limited” SE but the GBLC.

D. Q-DLTS measurement in the CCTO

Since the importance of the trap states for the CCTO was proposed from the conduction analysis in Sec. III C, Q-DLTS measurement is performed to further investigate the trap states and P-F emission in CCTO. The DLTS signal is defined as the charge released during the time interval from t_1 to t_2

$$\Delta Q = Q_0 \left[\exp\left(-\frac{t_1}{\tau}\right) - \exp\left(-\frac{t_2}{\tau}\right) \right], \quad (10)$$

where Q_0 is a constant, and τ is the time constant. When $\Delta Q = \Delta Q_{max}$, the τ is simply given by

$$\tau_m = (t_2 - t_1) / \ln(t_2/t_1). \quad (11)$$

In this study, $t_1 = 24, 36, 48, 72,$ and $96 \mu s$ from the point when the pulse voltage was removed and $t_2 = 10t_1$. Under these conditions, the trap level, ΔE_T can be described in terms of τ_m and temperature T as follows:^{55,56}

$$\tau_m^{-1} = \Gamma T^2 \exp\left(-\frac{\Delta E_T}{kT}\right), \quad (12)$$

where Γ is a material constant, and ΔE_T is the trap level below the conduction band. Fig. 11 shows the DLTS spectra of CCTO with several rate windows. We observe three

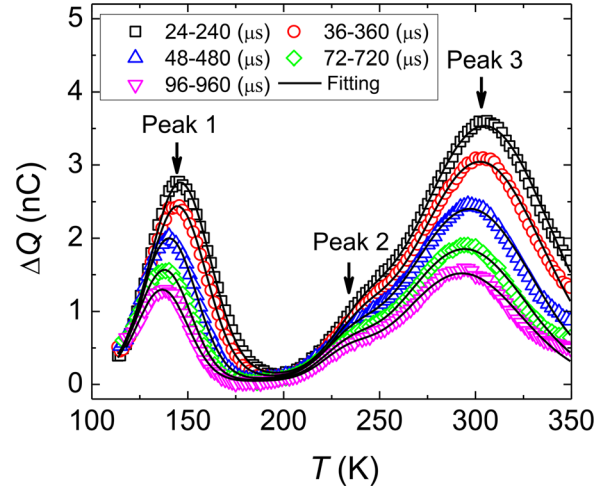


FIG. 11. DLTS spectra of CCTO. The gate time, t_1 and t_2 are shown in the inset with the ratio of $t_2/t_1 = 10$.

DLTS peaks from 100 to 350 K. ΔE_T for each peak can be obtained based on Eqs. (10) (12). Fig. 12 shows an inverse time constant Arrhenius plot corresponding to Eq. (12). ΔE_T was found to be 0.15, 0.79, and 0.66 eV for the peak 1, 2, and 3, respectively. The existence of the trap states, which is crucial for the formation of DSB, is elucidated. The number of trap states and their energy levels correspond well to reported values from the dielectric spectroscopy measurement.^{57,58} The trap level with $\Delta E_T = 0.15$ eV from peak 1 may be associated with the ionized donor level in the grain. Many studies have shown that the n-type grain (bulk) of CCTO have a small activation energy (~ 0.1 eV).^{5,10,59-61} The origin of the peak 2 is not clear. It could be from a specific point defect,⁶² adsorbed gas⁶³ as suggested in the other titanate materials, or defect dipoles, proposed in CCTO.^{6,7,64} Most importantly, the trap level with 0.66 eV from peak 3 is in very good agreement with our P-F analysis in Fig. 10. This proves that P-F conduction dominates the pre-breakdown regime in CCTO with the existence of trap state at $\Delta E_T = 0.66$ eV. The origin of this trap should be related to the secondary layers as discussed in Sec. III C. Moreover, the electronic trap states would have a significant influence

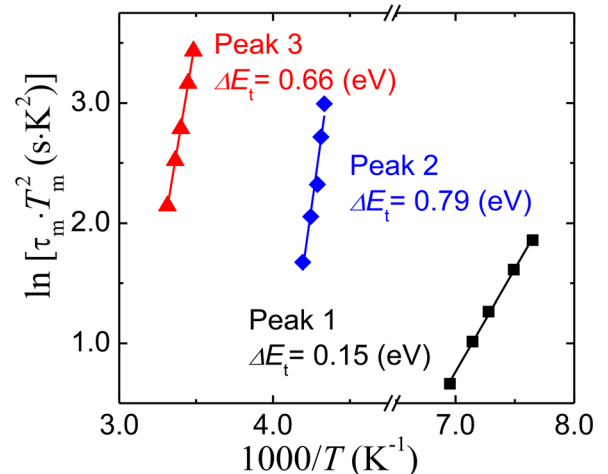


FIG. 12. Arrhenius plot of DLTS spectra of CCTO.

not only on the d.c. conduction, but also on the dielectric properties. It was reported that both the leakage current and $\tan \delta$ were remarkably improved due to the existence of P-F emission.⁵⁴ The $\tan \delta$ can be expressed as⁶⁵

$$\tan \delta = \frac{\epsilon''}{\epsilon'} = \frac{\epsilon_r'' + \sigma/\omega\epsilon_0}{\epsilon'}, \quad (13)$$

where ϵ'' , σ , and ω are real part and imaginary part of permittivity, conductivity, and angular frequency. Thus, the reduced σ would lead to low $\tan \delta$ at lower frequency.⁶⁵ According to Lee *et al.*, $\tan \delta$ was improved because the P-F emission with relatively deep trap center decreased σ .⁵⁴ This might be the case for our CCTO with IBLC structure. It is also reasonable to infer that the $\tan \delta$ is improved due to the increase in the depletion layer width. As can be understood from Eq. (9), the increase of negatively charged traps will increase the depletion layer width. In either case, the trap state should play an important role in the $\tan \delta$. In summary, *Q*-DLTS revealed three electronic trap states. One at $\Delta E_T = 0.66$ eV should be responsible for P-F conduction. In addition, it may affect $\tan \delta$ at a lower frequency by modifying the electronic state at DSB.

IV. CONCLUSIONS

The d.c. conduction of IBL system in the (1%Mn + 0.6%Nb)-doped STO and CCTO is demonstrated. The effective electric field at the grain boundary, E_{GB} , is estimated based on the SEM and *C-V* measurements. The d.c. conduction mechanism is discussed from the result of temperature dependence of *J-E_{GB}* characteristics. In both materials, three conduction mechanisms are suggested. Ohmic at the low E_{GB} , SE at the intermediate E_{GB} , and F-N tunneling at the high E_{GB} are suggested in the (1%Mn + 0.6%Nb)-doped STO. A new scaling law is introduced with the Schottky barrier height and depletion layer width for the prediction of the breakdown voltage. Whereas in contrast, *J-E_{GB}* characteristics of CCTO are more temperature dependent. CCTO is explained by an Ohmic conduction at the low E_{GB} , a P-F at the intermediate E_{GB} and SE at the high E_{GB} . The *Q*-DLTS measurements demonstrate that the trap center at $\Delta E_T = 0.66$ eV is responsible for the P-F conduction, which could result in a better insulation and lower $\tan \delta$. Although the macroscopic varistor-capacitor properties of the (1%Mn + 0.6%Nb) doped STO and CCTO can be explained by the DSB model, we have successfully shown that d.c. conduction of GBLC in two IBLC systems has distinct differences. We also hope that approaches and methodologies we have shown in this analysis can help many of the other conduction studies in various electroceramic systems.

ACKNOWLEDGMENTS

This work was supported by the National Science Foundation, as part of the Center for Dielectrics and Piezoelectrics under Grant No. IIP-1361571 and 1361503. Authors are grateful to Materials Characterization Lab staff at The Pennsylvania State University for their helpful discussions. K. Tsuji would like to thank the ITO Foundation for International Education Exchange for financial support.

W. T. Chen would like to thank MOST 104-2622-E-006-038-CC3 Ministry of Science and Technology R.O.C. for the financial support. Thanks to Dr. Bertrand Barbier for supplying some of the CCTO samples.

- ¹W. Heywang, *J. Am. Ceram. Soc.* **47**, 484 (1964).
- ²J. Bernasconi, S. Strassler, B. Knecht, H. P. Klein, and A. Menth, *Solid State Commun.* **21**, 867 (1977).
- ³M. Fujimoto, Y. M. Chiang, A. Roshko, and W. D. Kingery, *J. Am. Ceram. Soc.* **68**, 169 (1985).
- ⁴S. B. Desu and D. A. Payne, *J. Am. Ceram. Soc.* **73**, 3416 (1990).
- ⁵D. C. Sinclair, T. B. Adams, F. D. Morrison, and A. R. West, *Appl. Phys. Lett.* **80**, 2153 (2002).
- ⁶M. Whangbo and M. A. Subramanian, *Chem. Mater.* **18**, 3257 (2006).
- ⁷X. J. Luo, Y. S. Liu, C. P. Yang, S. S. Chen, S. L. Tang, and K. Barner, *J. Eur. Ceram. Soc.* **35**, 2073 (2015).
- ⁸C. C. Wang and L. W. Zhang, *Appl. Phys. Lett.* **88**, 042906 (2006).
- ⁹S. Krohns, P. Lunkenheimer, S. G. Ebbinghaus, and A. Loidl, *Appl. Phys. Lett.* **91**, 022910 (2007).
- ¹⁰T. B. Adams, D. C. Sinclair, and A. R. West, *Phys. Rev. B* **73**, 094124 (2006).
- ¹¹G. Zang, J. Zhang, P. Zheng, J. Wang, and C. Wang, *J. Phys. D: Appl. Phys.* **38**, 1824 (2005).
- ¹²Y. H. Lin, J. Cai, M. Li, C. W. Nan, and J. He, *J. Appl. Phys.* **103**, 074111 (2008).
- ¹³M. Li, Z. Shen, M. Nygren, A. Feteira, and D. C. Sinclair, *J. Appl. Phys.* **106**, 104106 (2009).
- ¹⁴R. Schmidt, M. C. Stennett, N. C. Hyatt, J. Pokorny, J. Prado Gonjal, M. Li, and D. C. Sinclair, *J. Eur. Ceram. Soc.* **32**, 3313 (2012).
- ¹⁵M. C. Ferrarelli, D. C. Sinclair, A. R. West, H. A. Dabkowska, A. Dabkowski, and G. M. Luke, *J. Mater. Chem.* **19**, 5916 (2009).
- ¹⁶C. C. Homes, T. Vogt, S. M. Shapiro, S. Wakimoto, and A. P. Ramirez, *Science* **293**, 673 (2001).
- ¹⁷D. Fu, H. Taniguchi, T. Taniyama, M. Itoh, and S. Koshihara, *Chem. Mater.* **20**, 1694 (2008).
- ¹⁸S. Y. Chung, *Chem. Mater.* **20**, 6284 (2008).
- ¹⁹S. H. Kim, H. W. Seon, H. T. Kim, J. G. Park, Y. Kim, and J. D. Byun, *Mater. Sci. Eng. B Solid State Mater. Adv. Technol.* **60**, 12 (1999).
- ²⁰M. Fujimoto, N. Yamaoka, and S. Shirasaki, *Jpn. J. Appl. Phys., Part 1* **26**, 1594 (1987).
- ²¹Y. Sato, T. Tanaka, F. Oba, T. Yamamoto, Y. Ikuhara, and T. Sakuma, *Sci. Technol. Adv. Mater.* **4**, 605 (2003).
- ²²S. H. Kim, J. H. Suh, J. G. Park, and Y. Kim, *Jpn. J. Appl. Phys., Part 1* **39**, 1788 (2000).
- ²³S. Y. Chung, J. H. Choi, and J. K. Choi, *Appl. Phys. Lett.* **91**, 091912 (2007).
- ²⁴J. F. Scott, M. Azuma, C. A. P. De Araujo, L. D. Mcmillan, M. C. Scott, and T. Roberts, *Integr. Ferroelectr.* **4**, 61 (1994).
- ²⁵H. Hu and S. B. Krupanidhi, *J. Mater. Res.* **9**, 1484 (1994).
- ²⁶S. M. Sze, *Physics of Semiconductor Devices*, 2nd ed. (Wiley, New York, 1981).
- ²⁷S. H. Yoon, S. H. Kim, and D. Y. Kim, *J. Appl. Phys.* **114**, 074102 (2013).
- ²⁸F. Chiu, *Adv. Mater. Sci. Eng.* **2014**, 578168.
- ²⁹L. Liu, L. Fang, Y. Huang, Y. Li, D. Shi, S. Zheng, S. Wu, and C. Hu, *J. Appl. Phys.* **110**, 094101 (2011).
- ³⁰L. M. Levinson and H. R. Philipp, *J. Appl. Phys.* **46**, 1332 (1975).
- ³¹G. W. Dietz and R. Waser, *Thin Solid Films* **299**, 53 (1997).
- ³²Y. W. Li, Y. D. Shen, Z. G. Hu, F. Y. Yue, and J. H. Chu, *Phys. Lett. A* **373**, 2389 (2009).
- ³³K. Tsuji, W. T. Chen, H. Guo, X. M. Chen, T. K. Lee, W. H. Lee, and C. A. Randall, *RSC Adv.* **6**, 92127 (2016).
- ³⁴B. Barbier, C. Combettes, S. Guillemet Fritsch, T. Chartier, F. Rossignol, A. Rumeau, T. Lebey, and E. Dutarde, *J. Eur. Ceram. Soc.* **29**, 731 (2009).
- ³⁵L. Marchin, S. Guillemet Fritsch, and B. Durand, *Prog. Solid State Chem.* **36**, 151 (2008).
- ³⁶M. A. L. Cordeiro, F. L. Souza, E. R. Leite, and A. J. C. Lanfredi, *Appl. Phys. Lett.* **93**, 182912 (2008).
- ³⁷T. Okamoto, J. Long, R. H. T. Wilke, J. Stitt, R. Maier, and C. A. Randall, *Jpn. J. Appl. Phys., Part 1* **55**, 026601 (2016).
- ³⁸K. Mukae, K. Tsuda, and I. Nagasawa, *J. Appl. Phys.* **50**, 4475 (1979).
- ³⁹W. Vaughan and W. G. Driscoll, *Handbook of Optics* (McGraw Hill, New York, 1978).

- ⁴⁰K. Mukae, K. Tsuda, and I. Nagasawa, *Jpn. J. Appl. Phys., Part 1* **16**, 1361 (1977).
- ⁴¹W. G. Morris, *J. Vac. Sci. Technol.* **13**, 926 (1976).
- ⁴²A. A. Felix, M. O. Orlandi, and J. A. Varela, *Solid State Commun.* **151**, 1377 (2011).
- ⁴³W. Wunderlich, H. Ohta, and K. Koumoto, *Phys. B Condens. Matter* **404**, 2202 (2009).
- ⁴⁴E. L. Murphy and R. H. Good, *Phys. Rev.* **102**, 1464 (1956).
- ⁴⁵S. Y. Chung, I. D. Kim, and S. J. L. Kang, *Nat. Mater.* **3**, 774 (2004).
- ⁴⁶Z. Y. Lu, X. M. Li, and J. Q. Wu, *J. Am. Ceram. Soc.* **95**, 476 (2012).
- ⁴⁷P. R. Bueno, M. A. Ramírez, J. A. Varela, and E. Longo, *Appl. Phys. Lett.* **89**, 191117 (2006).
- ⁴⁸M. A. Ramírez, P. R. Bueno, R. Tararam, A. A. Cavalheiro, E. Longo, and J. A. Varela, *J. Phys. D: Appl. Phys.* **42**, 185503 (2009).
- ⁴⁹A. P. Litvinchuk, C. L. Chen, N. Kolev, V. N. Popov, V. G. Hadjiev, M. N. Iliev, R. P. Bontchev, and A. J. Jacobson, *Phys. Status Solidi Appl. Res.* **195**, 453 (2003).
- ⁵⁰G. L. Li, Z. Yin, and M. S. Zhang, *Mater. Sci. Eng. B* **150**, 163 (2008).
- ⁵¹P. Fiorenza, R. Lo Nigro, C. Bongiorno, V. Raineri, M. C. Ferarrelli, D. C. Sinclair, and A. R. West, *Appl. Phys. Lett.* **92**, 182907 (2008).
- ⁵²L. Fang, M. Shen, and Z. Li, *J. Appl. Phys.* **100**, 104101 (2006).
- ⁵³S. Y. Lee, S. M. Choi, M. Y. Kim, S. I. Yoo, J. Hye Lee, W. Jo, Y. H. Kim, and K. J. Choi, *J. Mater. Res.* **26**, 2543 (2011).
- ⁵⁴S. Y. Lee, H. E. Kim, W. Jo, Y. H. Kim, and S. I. Yoo, *Electron. Mater. Lett.* **11**, 1003 (2015).
- ⁵⁵K. I. Kirov and K. B. Radev, *Phys. Status Solidi* **63**, 711 (1981).
- ⁵⁶J. W. Farmer, C. D. Lamp, and J. M. Meese, *Appl. Phys. Lett.* **41**, 1063 (1982).
- ⁵⁷K. Barner, X. J. Luo, X. P. Song, C. Hang, S. S. Chen, I. V. Medvedeva, and C. P. Yang, *J. Mater. Res.* **26**, 36 (2011).
- ⁵⁸R. Jia, J. Li, L. Hou, and H. Li, in *2015 IEEE 11th International Conference on Properties and Applications of Dielectric Materials* (2015), pp. 836–839.
- ⁵⁹J. L. Zhang, P. Zheng, C. L. Wang, M. L. Zhao, J. C. Li, and J. F. Wang, *Appl. Phys. Lett.* **87**, 142901 (2005).
- ⁶⁰M. Li, A. Feteira, D. C. Sinclair, and A. R. West, *Appl. Phys. Lett.* **88**, 232903 (2006).
- ⁶¹D. L. Sun, A. Y. Wu, and S. T. Yin, *J. Am. Ceram. Soc.* **91**, 169 (2007).
- ⁶²Y. M. Chiang and T. Takagi, *J. Am. Ceram. Soc.* **73**, 3286 (1990).
- ⁶³Y. Nakano and N. Ichinose, *J. Mater. Res.* **5**, 2910 (1990).
- ⁶⁴X. J. Luo, C. P. Yang, S. S. Chen, X. P. Song, H. Wang, and K. Barner, *J. Appl. Phys.* **108**, 014107 (2010).
- ⁶⁵S. Guillemet Fritsch, T. Lebey, M. Boulos, and B. Durand, *J. Eur. Ceram. Soc.* **26**, 1245 (2006).